17th World Conference on Earthquake Engineering, 17WCEE
Sendai, Japan - September 13th to 18th 2020

EXPERIMENTAL INVESTIGATION ON MECHANICAL PERFORMANCE OF A CRANK INERTER

R.F. Zhang[(1)], L. Zhang[(2)], L.F. Hao[(3)], S.T. Xue[(4)]

[(1)] *Associate Professor, Department of Disaster Mitigation for Structures, Tongji University, Shanghai 200092, China, zhangruifu@tongji.edu.cn*
[(2)] *PhD candidate, Department of Disaster Mitigation for Structures, Tongji University, Shanghai 200092, China, zhangli24@tongji.edu.cn*
[(3)] *Assistant Professor, Earthquake Engineering Research & Test Center, Guangzhou University, Guangzhou 510405, China, haolf@gzhu.edu.cn*
[(4)] *Professor, Department of Disaster Mitigation for Structures, Tongji University, Shanghai 200092, China, xue@tongji.edu.cn*

Abstract

The inerter has been proven to be effective for structural vibration mitigation, which is capable of generating apparent mass effect known as inertance. However, the complicated configuration of the existing inerter elements may limit its application. In this study, a crank inerter is proposed based on a simple crank mechanism, which can transform the translational motion of the axial motion into the rotational motion of flywheel. The configuration and corresponding mathematical model of the inerter element are firstly introduced. The inertance of crank inerter is nonlinear and related to the amplitude of the translational motion. A dynamic test was conducted to verify the mathematical model and the nonlinear inertance of this inerter element under sinusoidal excitations. The experimental data show that the theoretical model is consistent with the actual model and the proposed inerter element can achieve the expected inertance.

Keywords: crank inerter; nonlinear inertance; vibration control;

1 Introduction

The inerter system is proven to be feasible and effective for structural vibration suppression [1, 2]. A typical inerter system usually consists of the inerter element, spring element and damping element [3]. As a key mechanical element in the inerter system, the inerter is considered as a two-terminal mass element with the apparent mass effect [1, 4]. With these characteristics, the inerter has been of great interest to many scholars.

Previous scholars have proposed different types of physical realization mechanisms for inerter elements. By using the hydraulic mechanism, a mass pump, which utilizes the inertance of liquid with two-terminal connection, is proposed for the structural vibration control in 1970s [5]. In 2000s, the ball screw mechanism was employed by Saito et al. [6, 7] and Ikago et al. [1] to fabricate the inerter element and thousands of times of the apparent mass was obtained with small physical mass. The inerter utilizing rack-and-pinion was proposed and analyzed by Smith [8] to obtain the inertance. Based on the electromagnetic mechanism, an inerter-based device is introduced by Gonzales-Buelga [9] using an electromagnetic transducer. For engineering design and application, however, the existing inerter still have the shortcoming such as complicated configuration.

This study proposes a novel inerter element using the simple crank mechanism to obtain the apparent mass. The configuration of crank inerter is given and the mathematical model of crank inerter is derived. The nonlinear inertance is obtained with crank inerter under dynamic excitation. A prototype crank inerter is designed and fabricated for experimental research. The dynamic test on crank inerter is conducted to verify the mathematical model and analyze the inertance of crank inerter.

2 Configuration of crank inerter

The configuration of the crank mechanism is shown in Fig. 1, where r and l denote the length of the crank *OA* and rod *AB*, respectively, and R is the radius of the flywheel. The distance between the points *O* and *B* is denoted as x_B. The angle between *OA* and *OB* is denoted as φ, while β denotes the angle between *OB* and *AB*. Under the external excitation F_z, the linear motion of the slider can be transferred to the rotational motion of the flywheel with the crank mechanism, which is the key point for achieving the apparent mass effect characterized by the inerter. In this study, the crank is employed to drive the rotation of the flywheel in an inerter element, which is called the crank inerter, as shown in Fig. 1.

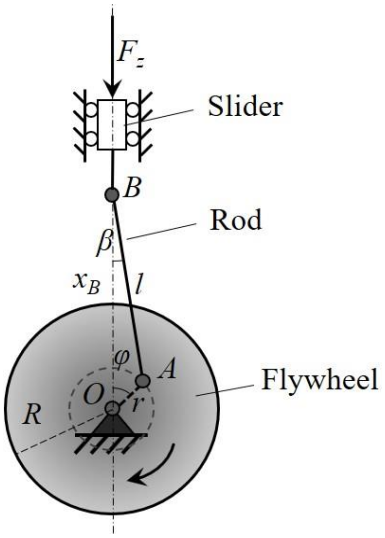

Fig. 1 Schematic diagram of crank inerter

3 Mechanical model

To obtain the working mechanism of crank inerter, the kinematic analysis is conducted herein. As is shown in Fig. 1, x_B can be calculated as

$$x_B = r\cos\varphi + l\cos\beta \tag{1}$$

The geometrical relationship between angles φ and β can be expressed as

$$r\sin\varphi = l\sin\beta \tag{2}$$

Substituting Eq. (2) into Eq. (1), x_B can be rewritten as

$$x_B = r\cos\varphi + \sqrt{l^2 - r^2\sin^2\varphi} \tag{3}$$

With the cosine theorem, $\cos\varphi$ can be calculated in $\triangle$AOB as follows:

$$\cos\varphi = \frac{x_B^2 + r^2 - l^2}{2x_B r} \tag{4}$$

Then, φ can be expressed as

$$\varphi = \cos^{-1}\left(\frac{x_B^2 + r^2 - l^2}{2x_B r}\right) \tag{5}$$

Taking the first and second derivates of both φ and x_B with respect to time t in both sides of Eq. (4), the angular velocity $\dot{\varphi}$ and angular acceleration $\ddot{\varphi}$ can be calculated as

$$\dot{\varphi} = \frac{r^2 - x_B^2 - l^2}{2rx_B^2 \cdot \sin\varphi}\dot{x}_B \tag{6}$$

$$\ddot{\varphi} = \frac{1}{\sin\varphi}\cdot\left[\frac{2\left(l^2 - r^2\right)\cdot\dot{x}_B^2 + \left(r^2 - l^2 - x_B^2\right)x_B\cdot\ddot{x}_B}{2rx_B^3} - \dot{\varphi}\cos\varphi\right] \tag{7}$$

where $\dot{x}_B$ and $\ddot{x}_B$ are the velocity and acceleration of the linear motion rod of crank inerter, respectively.

Under the external excitation F_z, the transfer of forces in crank inerter is plotted as Fig. 2. Assuming that the reciprocating inertia force of the linear motion rod is ignored in the force analysis due to its small mass compared to the flywheel, the force F_z equals to the summation of the friction force F_f and the force F along the linear motion rod. The force F can be devided into the lateral pression F_c of the guide and the force F_l along the connecting rod. And F_l can be devided into the radial force F_n and the tangential force F_t. The rotation of the flywheel in crank inerter is driven by the tangential force F_t.

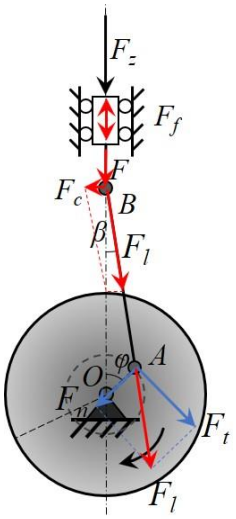

Fig.2 Relationships between forces in crank inerter

The friction force F_f can be calculated as

$$F_f = -\mu F_c \operatorname{sgn}(\dot{x}_B) \tag{8}$$

$$\operatorname{sgn}(\dot{x}_B) = \begin{cases} 1 & ,\dot{x}_B > 0 \\ 0 & ,\dot{x}_B = 0 \\ -1 & ,\dot{x}_B < 0 \end{cases} \tag{9}$$

where μ is the coefficient of friction.

According to the parallelogram rule of force, F_c and F_l can be respectively calculated as follows:

$$F_c = F \tan\beta \tag{10}$$

$$F_l = F / \cos\beta \tag{11}$$

Deviding the force F_l, we can express the forces F_n and F_t as

$$F_n = F \cos(\phi + \beta) / \cos\beta \tag{12}$$

$$F_t = F \sin(\phi + \beta) / \cos\beta \tag{13}$$

According to the moment equilibrium priciple of the flywheel with respect to the point *O*, F_t needs to satisfy the expression as follows:

$$I_m \ddot{\varphi}(t) = F_t r = Fr \sin(\phi + \beta) / \cos\beta \tag{14}$$

where $I_m = m_1 r^2 / 2$ is the moment of inertia of the flywheel with the mass m_1. Then, the force F can be rewritten as follows:

$$F = \frac{mR^2 \ddot{\varphi}(t) \cos\beta}{2r \sin(\phi + \beta)} \tag{15}$$

For the two-terminal inerter element, the inertance m_{in} is considered as the key parameter and defined as the ratio of the force of inerter to the relative acceleration between two nodes of inerter. In a common inerter device, such as the inerter using ball-screw or rack-and-pinion mechanism, the inertance m_{in} is usually constant when the size of an inerter is determined. Substituting Eqs. (3), (6) and (7) into Eq. (15), the ratio of the force F to $\ddot{x}_B$ is a funtion of the angle φ and the angular velocity $\dot{\varphi}$, which are both related to the value of x_B. That means, ignoring the friction force, the inertance m_{in} is nonlinear and not constant in a crank inerter with determined size. The nonlinear m_{in} of crank inerter may be beneficial to the vibration control on a wider bandwidth of excitation frequency compared to the constant inertance.

4 Experimental illustration

In order to obtain the mechanical behavior and confirm the mathematical model of crank inerter derived above, a prototype device is designed and manufactured for experimental research under sinusoidal excitations as shown in Fig. 3. The specifications of crank inerter are listed in Table 1. The stroke of crank inerter is ±15 mm. A hydraulic actuator as well as the built-in displacement sensor is employed in testing crank inerter. A load cell is placed at the end of actuator to measure the force response as shown in Fig. 3. The force and frequency range of the actuator are 0-15 kN and 0-10 Hz, respectively. The sinusoidal excitations are generated with the displacement control mode. The displacement and force responses are recorded by the data logger with the sampling frequency of 1000 Hz. These responses are filtered by a low-pass Butterworth filter with a cutoff frequency of 10 Hz to remove the interference of high frequency signal. In all of the crank inerter testing cases, the initial loading place is set at where φ equals to $\pi/2$.

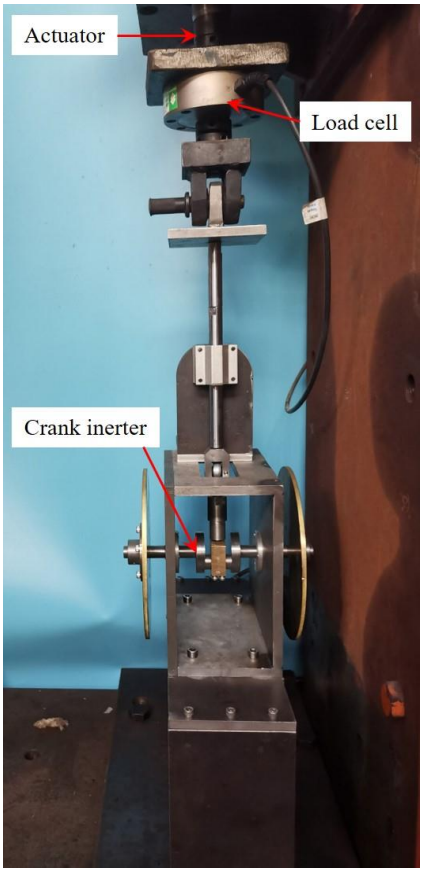

Fig. 3 Photograph of experimental setup for crank inerter test

Table 1 Specifications of crank inerter in the dynamic test

Parameter of crank inerter	Value
Length of connecting rod l (mm)	100
Length of crank r (mm)	15
Radius of flywheel R_0 (mm)	100
Radius of flange R_1 (mm)	40

According to the mathematical derivations, the inertance of crank inerter is related to the angle φ and angular velocity $\dot{\varphi}$ of crank. Both the ranges of $\dot{\varphi}$ and φ are related to the loading amplitude. Hence, the mechanical behaviors of crank inerter are tested under certain frequency sinusoidal excitations with variable amplitudes of 10 mm, 11 mm, 12 mm and 13 mm.

5 Discussion

In this section, the output forces of crank inerter obtained through the experimental data and the mechanical formulas are compared to verify the derivations above. The nonlinear property of crank inerter is also analyzed under the sinusoidal excitations with different frequencies and amplitudes.

Using the specifications of crank inerter listed in Table 1, the time history response of φ can be obtained under the sinusoidal excitations. Then, assuming that the friction force F_f can be ignored due to both F_c and μ are small, the output force of crank inerter can be numerically obtained with Eq. (15). Under the sinusoidal excitation with frequency of 2 Hz and amplitude of 10 mm, the comparison between the experimental and theoretical results of the force of crank inerter is shown in Fig. 4(a). It can be seen that the tendency of theoretical value matches well with the experimental value of the force of crank inerter. The peak value of the experimental force is larger than theoretical force of crank inerter. This is mainly due to the neglect of friction force in theoretical analysis. Fig. 4(b) compares the hysteretic loops of theoretical and experimental results of crank inerter. It can be seen that the experimental result shows slightly energy dissipation effect in one cycle because of the friction. The nonlinear behavior of crank inerter can be obviously observed with a nonlinear hysteretic loop, which is different with a common inerter element with a slanted linear hysteretic loop.

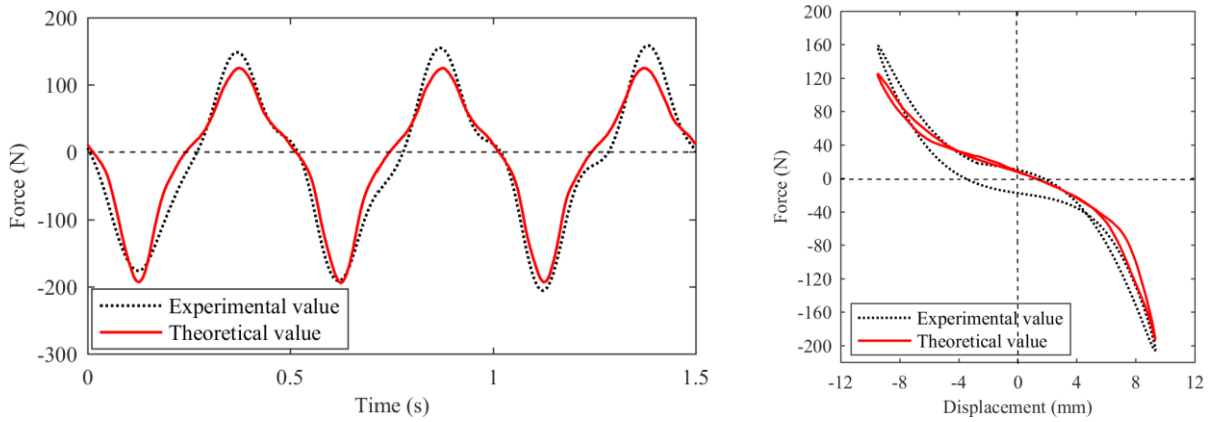

(a) Force versus time (b)Force versus displacement

Fig. 4 Comparisons between experimental and theoretical results for crank inerter under sinusoidal excitation (frequency: 2Hz, amplitude: 10 mm)

The mechanical behaviors of crank inerter are also checked under 2 Hz sinusoidal excitations with variable amplitudes of 11 mm, 12 mm and 13 mm. The corresponding hysteretic behaviors of crank inerter are shown in Fig. 5. The theoretical value of crank inerter is not very consistent with experimental value of crank inerter under 2 Hz sinusoidal excitation with amplitude of 13 mm. For this testing case, the output force of crank inerter is relatively large, which can cause a large lateral pression F_c of the guide. Hence, the friction force F_f is the main factor for the difference between the theoretical and experimental value of crank inerter. This also explains the obvious energy dissipation effect for the testing case of 13 mm amplitude. Furthermore, it can be seen that the maximum output force of crank inerter increases rapidly with the increasing of excitation amplitude under a certain frequency excitation, and the maximum force of crank inerter is occured at moment of the maximum displacement. This means, the inertance m_{in} of crank inerter at the maximum amplitude also increases rapidly. The nonlinear characteristic of crank inerter is also more obvious for a large amplitude. Under 2 Hz sinusoidal excitations for amplitudes of 10 mm, 11 mm, 12 mm and 13 mm, the inertance m_{in} of crank inerter at the maximum amplitude is calculated with $m_{in} = F / \left[-(2\pi f)^2 A \right]$ according to the experimental and theoretical results, as listed in Table 2. It can be seen, for a 3 mm amplitude increase of the sinusoidal excitation (i.e., from A=10mm to A=13mm), the inertance m_{in} of crank inerter can increase by more than 3 times. This characteristic may be beneficial to the vibration control for structures with large displacement response.

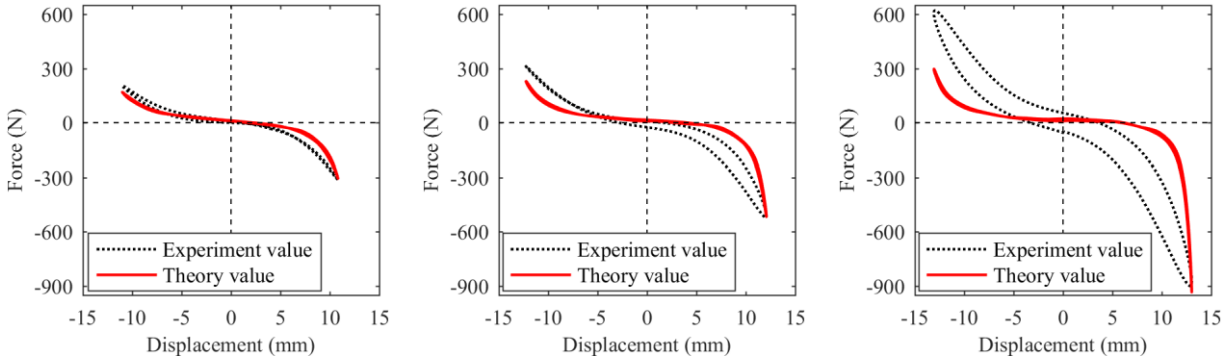

(a) Amplitude=11 mm (b) Amplitude=12 mm (c) Amplitude=13 mm

Fig. 5 Hysteretic behaviors of crank inerter under 2 Hz sinusoidal excitations with different amplitudes

Table 2 m_{in} of crank inerter under 2 Hz sinusoidal excitations with different amplitudes

	A=10 mm	A=11 mm	A=12 mm	A=13 mm
Experimental result of m_{in} (kg)	141.1	185.5	271.9	424.0
Theoretical result of m_{in} (kg)	132.5	181.8	269.9	440.7

The time history response of angular accelerations $\ddot{\varphi}$ of crank inerter under 2 Hz sinusoidal excitations with different amplitudes are checked to explain the rapid increase of the maximum output force of crank inerter, as shown in Fig. 6. It can be seen the peak value of the negative $\ddot{\varphi}$ decreases rapidly with the increasing of the excitation amplitude, which accounts for the rapid increase of the force and inertance of crank inerter. Note that the symmetry of the force with respect to zero is related to the initial crank position. The initial loading place of $\varphi = \pi/2$ set in this study is not the middle position for obtaining a symmetrical output force for of crank inerter under sinusoidal excitation.

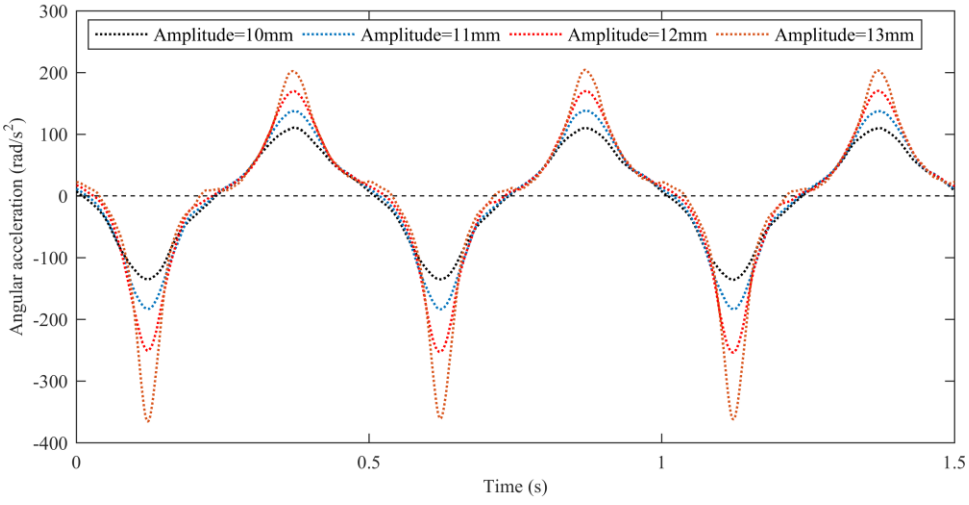

Fig. 6 Hysteretic behaviors of crank inerter with different excitation frequency

6 Conclusion

An inerter element using crank mechanism is proposed for structural vibration control. . The conclusions can be drawn as follows:

(1) The mechanical model of crank inerter is verified with the experimental result, and when the output force of crank inerter is large (e.g., under the large amplitude sinusoidal excitation), however the influence of friction of the guide in crank inerter should not be neglected.

(2) The inertance of crank inerter is nonlinear and related to the crank rotational angle φ and angular velocity $\dot{\varphi}$ of crank under the external dynamic excitations.

(3) The nonlinear property of crank inerter is more obvious under a larger amplitude sinusoidal excitation. This characteristic is beneficial to the structural vibration control with large displacement response.

Acknowledgement

This study was supported by the National Natural Science Foundation of China (Grant 51978525, 51778490 and 51908156), and the Key Program for International S&T Cooperation Projects of China (No.2016YFE0127600).

References

[1] Ikago K, Saito K, Inoue N (2012): Seismic control of single-degree-of-freedom structure using tuned viscous mass damper. *Earthquake Engineering & Structural Dynamics*, 41, 453-474.

[2] Pan C, Zhang RF (2018): Design of structure with inerter system based on stochastic response mitigation ratio. *Structural Control & Health Monitoring*, 25, e2169.

[3] Pan C, Zhang R, Luo H, Li C, Shen H (2018): Demand-based optimal design of oscillator with parallel-layout viscous inerter damper. *Structural Control & Health Monitoring*, 25, e2051.

[4] Zhang RF, Zhao ZP, Pan C, Ikago K, Xue ST (2020): Damping enhancement principle of inerter system. *Structural Control and Health Monitoring*. DOI:10.1002/stc.2523.

[5] Kawamata S (1973): Development of a vibration control system of structures by means of mass pumps. *Technical Report 1973*, Institute of Industrial Science, University of Tokyo, Tokyo, Japan.

[6] Saito K, Sugimura Y, Nakaminami S, Kida H, Inoue N (2008): Vibration tests of 1-story response control system using inertial mass and optimized soft spring and viscous element. *Proceedings of the 14th World Conference on Earthquake Engineering*, Beijing, China.

[7] Saito K, Yogo K, Sugimura Y, Nakaminami S, Park K (2004): Application of rotary inertia to displacement reduction for vibration control system. *13th World Conference on Earthquake Engineering*, Vancouver, Canada.

[8] Smith MC (2002): Synthesis of mechanical networks: the inerter. *IEEE Transactions on Automatic Control*, 47, 1648-1662.

[9] Gonzalez-Buelga A, Clare L, Neild S, Jiang J, Inman D (2015): An electromagnetic inerter-based vibration suppression device. *Smart Materials and Structures*, 24, 055015.

